Atmos. Meas. Tech., 15, 6935–6947, 2022
https://doi.org/10.5194/amt-15-6935-2022

Atmospheric Measurement Techniques
Open Access
EGU

Online measurements of cycloalkanes based on NO^+ chemical ionization in proton transfer reaction time-of-flight mass spectrometry (PTR-ToF-MS)

Yubin Chen[1,2], Bin Yuan[1,2], Chaomin Wang[3], Sihang Wang[1,2], Xianjun He[1,2], Caihong Wu[1,2], Xin Song[1,2], Yibo Huangfu[1,2], Xiao-Bing Li[1,2], Yijia Liao[1,2], and Min Shao[1,2]

[1]Institute for Environmental and Climate Research, Jinan University, Guangzhou 511443, China
[2]Guangdong-Hongkong-Macau Joint Laboratory of Collaborative Innovation for Environmental Quality, Guangzhou 511443, China
[3]School of Tourism and Culture, Guangdong Eco-engineering Polytechnic, Guangzhou 510520, China

Correspondence: Bin Yuan (byuan@jnu.edu.cn)

Received: 5 September 2022 – Discussion started: 6 September 2022
Revised: 15 November 2022 – Accepted: 17 November 2022 – Published: 2 December 2022

Abstract. Cycloalkanes are important trace hydrocarbons existing in the atmosphere, and they are considered a major class of intermediate volatile organic compounds (IVOCs). Laboratory experiments showed that the yields of secondary organic aerosols (SOAs) from oxidation of cycloalkanes are higher than acyclic alkanes with the same carbon number. However, measurements of cycloalkanes in the atmosphere are still challenging at present. In this study, we show that online measurements of cycloalkanes can be achieved using proton transfer reaction time-of-flight mass spectrometry with NO^+ chemical ionization (NO^+ PTR-ToF-MS). Cyclic and bicyclic alkanes are ionized with NO^+ via hydride ion transfer, leading to major product ions of $C_nH_{2n-1}^+$ and $C_nH_{2n-3}^+$, respectively. As isomers of cycloalkanes, alkenes undergo association reactions with major product ions of $C_nH_{2n} \cdot (NO)^+$, and concentrations of 1-alkenes and *trans*-2-alkenes in the atmosphere are usually significantly lower than cycloalkanes (about 25 % and < 5 %, respectively), as a result inducing little interference with cycloalkane detection in the atmosphere. Calibrations of various cycloalkanes show similar sensitivities associated with small humidity dependence. Applying this method, cycloalkanes were successfully measured at an urban site in southern China and during a chassis dynamometer study of vehicular emissions. Concentrations of both cyclic and bicyclic alkanes are significant in urban air and vehicular emissions, with comparable cyclic alkanes / acyclic alkanes ratios between urban air and gasoline vehicles. These results demonstrate that NO^+ PTR-ToF-MS provides a new complementary approach for the fast characterization of cycloalkanes in both ambient air and emission sources, which can be helpful to fill the gap in understanding the importance of cycloalkanes in the atmosphere.

1 Introduction

Organic compounds, as important trace components in the atmosphere, are released into the atmosphere from many different natural and anthropogenic sources, which have complicated and diverse chemical compositions (de Gouw, 2005; Goldstein and Galbally, 2007; He et al., 2022). Components and concentration levels of organic compounds largely affect atmospheric chemistry, atmospheric oxidation capacity, and radiation balance (Monks et al., 2015; Wu et al., 2020), as well as human health (Xing et al., 2018). According to effective saturation concentrations (Donahue et al., 2012), organic compounds can be divided into intermediate volatile organic compounds (IVOCs), semi-volatile organic compounds (SVOCs), low volatile organic compounds (LVOCs), and extremely low volatile organic compounds (ELVOCs). Due to high yields of secondary organic aerosol (SOA) (Lim and Ziemann, 2009; Robinson et al., 2007), IVOCs have been

proved to be important SOA precursors in urban atmospheres (Tkacik et al., 2012; Zhao et al., 2014).

Many studies have shown higher alkanes (i.e., linear and branched alkanes with 12–20 carbon atoms) to be important chemical components of IVOCs (Li et al., 2019; Zhao et al., 2014). Similarly to these acyclic alkanes, cycloalkanes can also account for significant fractions of IVOCs. Cycloalkanes can reach more than 20 % of IVOC concentrations in diesel vehicle exhausts, lubricating oil, and diesel fuels (Alam et al., 2018; Liang et al., 2018; Lou et al., 2019), which are comparable to or even higher than linear and branched alkanes. In some oil and gas regions, high concentrations of cycloalkanes have also been reported (Aklilu et al., 2018; Gilman et al., 2013; Warneke et al., 2014). More importantly, laboratory studies suggest that SOA yields of cyclic and polycyclic alkanes are significantly higher than linear or branched alkanes with the same carbon number (as high as a factor of 5) (Hunter et al., 2014; Jahn et al., 2021; J. Li et al., 2021; Loza et al., 2014; Yee et al., 2013). As a result, cyclic and bicyclic species are shown to be large contributors to SOA formation potential from vehicles (Xu et al., 2020a, b; Zhao et al., 2015, 2016). Recently, Hu et al. (2022) proposed that IVOC contributions to SOA formation in an urban region can increase from 8 %–20 % (acyclic alkanes only) to 17.5 %–46 % if cycloalkanes are considered, signifying the importance of cycloalkanes in SOA formation.

Cycloalkanes are mainly measured using gas chromatography–mass spectrometry/flame ionization detector (GC-MS/FID) and two-dimensional gas chromatography techniques (GC × GC) (Alam et al., 2018, 2016; de Gouw et al., 2017; Liang et al., 2018; Zhao et al., 2016). Based on measurements of gas chromatographic techniques, the signals of unspeciated cyclic compounds can be determined. This is done by subtracting the total signal for each retention time bin according to the series of n-alkanes (Zhao et al., 2014, 2016). The mass of linear alkanes and branched alkanes in each bin is calculated by using the total ion current (TIC) and the fraction of characteristic fragments ($C_4H_9^+$, m/z 57) (Zhao et al., 2014, 2016). However, this type of quantitative method does not explicitly distinguish individual cycloalkanes, and the determined mass may contain other cyclic compounds, e.g., polycyclic aromatic hydrocarbons and compounds containing oxygen or multifunctional groups (Zhao et al., 2014, 2015, 2016). Due to the need for collection and pretreatment of air samples, time resolution of GC-MS techniques is usually in the range of 0.5–1.0 h or above.

Proton transfer reaction mass spectrometry (PTR-MS) using hydronium ions (H_3O^+) as the reagent ion is capable of measuring many organic compounds with a high response time and sensitivity (de Gouw and Warneke, 2007; Yuan et al., 2017). However, detection of alkanes and cycloalkanes using PTR-MS with H_3O^+ ionization is challenging, as usually only a series of fragment ions ($C_nH_{2n+1}^+$, $C_nH_{2n-1}^+$, $n \geq 3$) are observed (Erickson et al., 2014; Gueneron et al., 2015). Recently, it was demonstrated that linear alkanes can be measured by PTR-MS with a time-of-flight detector using NO^+ as reagent ions (NO^+ PTR-ToF-MS) (Inomata et al., 2014; Koss et al., 2016; Wang et al., 2020). These higher alkanes are ionized by NO^+ via hydride ion transfer, leading to major product ions of $C_nH_{2n+1}^+$, with a low degree of fragmentation (Inomata et al., 2014). Meanwhile, it is interesting that cycloalkanes were also quantified using $C_nH_{2n+1}^+$ ions in H_3O^+ PTR-MS in oil and gas regions (Koss et al., 2017; Warneke et al., 2014; Yuan et al., 2014), though sensitivities were substantially low (∼ 10 % of other species) (Warneke et al., 2014). This evidence suggests that the NO^+ ionization scheme could provide a possibility for measuring cycloalkanes along with acyclic alkanes, as demonstrated in two recent works (Koss et al., 2016; Wang et al., 2022a).

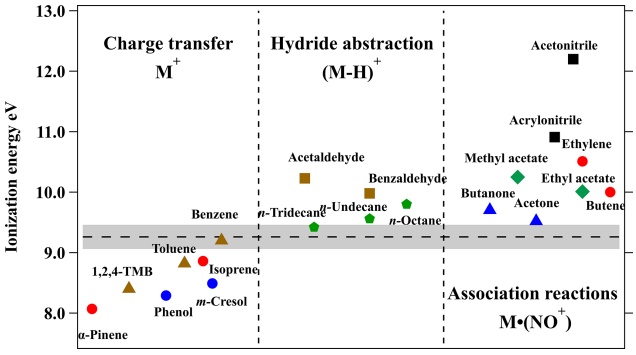

Figure 1. Ionization energy (IE) and reaction pathways with NO^+ ions of organic compounds including alkanes (green pentagon), aromatics (brown triangle), alkenes (red circle), phenolic species (blue circle), aldehydes (brown square), ketones (blue triangle), esters (green diamond), and nitrogen-containing species (black square). The ionization energy of NO (9.26 eV) is represented by the dashed line, with shading representing reported uncertainty. The IE of various organic compounds can be obtained in the NIST Chemistry WebBook (http://webbook.nist.gov, last access: 29 November 2022). The abbreviation "1,2,4-TMB" corresponds to 1,2,4-trimethylbenzene.

In this study, we discuss the potential of online measurements of cycloalkanes for ambient air and emission sources utilizing NO^+ ionization in PTR-ToF-MS. The results of laboratory experiments to characterize product ions, calibration, and response time will be shown. Finally, measurements of cycloalkanes using NO^+ PTR-ToF-MS will be demonstrated from deployments at an urban site in southern China and a chassis dynamometer study for vehicular emissions.

2 Methods

2.1 NO^+ PTR-ToF-MS measurements

A commercial PTR-ToF-MS instrument (Ionicon Analytik, Austria) equipped with a quadrupole ion (Qi) guide for effective transfer of ions from the drift tube to the time-of-flight

Table 1. The formula, purity, and ionization energy (IE) of the species used in product ion characterization experiments are shown. The percentage of each product ion from the reactions with NO^+ ions is indicated in parentheses, and the major product ions are identified in bold.

Species	Formula	Purity (%)	IE[a] (eV)	Product ions (%)		
Cycloheptane	C_7H_{14}	98.0 %	9.82	**$C_7H_{13}^+$(100)**		
Methylcyclohexane	C_7H_{14}	99.0 %	9.64	**$C_7H_{13}^+$(100)**		
Cyclododecane	$C_{12}H_{24}$	99.0 %	9.72	**$C_{12}H_{23}^+$(82)**	$C_8H_{15}^+$(8)	$C_7H_{13}^+$(10)
Hexylcyclohexane	$C_{12}H_{24}$	98.0 %	N/A[b]	**$C_{12}H_{23}^+$(79)**	$C_8H_{15}^+$(10)	$C_7H_{13}^+$(11)
Cyclopentadecane	$C_{15}H_{30}$	98.0 %	N/A[b]	**$C_{15}H_{29}^+$(77)**	$C_7H_{13}^+$(7)	$C_8H_{15}^+$(< 5)
				$C_9H_{17}^+$(< 5)	$C_{10}H_{19}^+$(< 5)	$C_{11}H_{21}^+$(< 5)
				$C_{15}H_{30}^+$(6)		
Nonylcyclohexane	$C_{15}H_{30}$	98.0 %	N/A[b]	**$C_{15}H_{29}^+$(74)**	$C_7H_{13}^+$(19)	$C_8H_{15}^+$(< 5)
				$C_9H_{17}^+$(< 5)	$C_{10}H_{19}^+$(< 5)	$C_{11}H_{21}^+$(< 5)
Bicyclohexyl	$C_{12}H_{22}$	99.0 %	9.41	**$C_{12}H_{21}^+$(71)**	$C_5H_{11}^+$(17)	$C_5H_{13}^+$(< 5)
				$C_7H_{13}^+$(5)	$C_8H_{15}^+$(< 5)	$C_{12}H_{22}^+$(< 5)
1-Heptene	C_7H_{14}	99.5 %	9.34	**$C_7H_{13}HNO^+$(40)**	$C_5H_9HNO^+$(15)	$C_{12}H_{22}^+$(< 5)
				$C_3H_5HNO^+$(< 5)	C_7H14^+(< 5)	$C_4H_7HNO^+$(37)
1-Decene	$C_{10}H_{20}$	99.5 %	9.42	**$C_{10}H_{19}HNO^+$(51)**	$C_5H_9HNO^+$(18)	$C_6H_{11}HNO^+$(15)
				$C_4H_7HNO^+$(12)	$C_{10}H_{19}^+$(< 5)	$C_7H_{13}HNO^+$(< 5)
				$C_{10}H_{20}^+$(< 5)		

[a] NIST Chemistry WebBook (http://webbook.nist.gov, last access: 29 November 2022). [b] N/A stands for "not available".

mass spectrometer is used for this work (Sulzer et al., 2014), and the mass resolution reaches approximately $3000\,m/\Delta m$ (Fig. S1 in the Supplement). In order to generate NO^+ ions, 5 sccm ultra-high-purity air (O_2+$N_2 \geq 99.999$ %) is directed into the hollow cathode discharge area of the ion source; NO^+ ions are produced by ionization as follows (Federer et al., 1985; Karl et al., 2012):

$$N^+ + O_2 \rightarrow NO^+ + O, \quad \text{(R1)}$$

$$O^+ + N_2 \rightarrow NO^+ + N, \quad \text{(R2)}$$

$$N_2^+ + O_2 \rightarrow O_2^+ + N_2, \quad \text{(R3)}$$

$$O_2^+ + NO \rightarrow NO^+ + O_2. \quad \text{(R4)}$$

For the purpose of ionizing NO^+ ions to the greatest extent and reducing the generation of impurity ions such as H_3O^+, O_2^+, and NO_2^+, the ion source voltages U_S and U_{SO} was set to 40 and 100 V, while drift tube voltages U_{dx} and U_{drift} were set to 23.5 and 470 V with drift tube pressure at 3.8 mbar, resulting in an E/N (electric potential intensity relative to gas number density) of 60 Td. The specific details have been described in Wang et al. (2020). The intensities of primary ions NO^+ and impurities including O_2^+, NO_2^+, and $H_3O^+$and the ratio of O_2^+ to NO^+ during the measurements of urban air and vehicular emissions are shown in Fig. S2. The abundances of O_2^+, NO_2^+, and H_3O^+ are significantly lower than NO^+ ions, and the ratio of O_2^+ to NO^+ is basically below 5 % during the measurements of urban air except for the period of 26 October to 2 November 2018 (7 %–10 %), while the ratio of O_2^+/NO^+ is basically below 2 % during the measurements of vehicular emissions. The measured ToF data are processed for high-resolution peak fitting using Tofware (Tofwerk AG, version 3.0.3), obtaining high-precision signals for cycloalkanes (Fig. S3). The signal of cycloalkanes used for quantification has been subtracted from the contribution of isotopes of other ions and other species such as unsaturated aldehydes that share an identical formula at the unit mass resolution (UMR) with cycloalkanes during the high-resolution peak fitting process. A description of the fitting and calculation methods have been fully discussed in previous studies (Stark et al., 2015; Timonen et al., 2016). The raw ion count signals of NO^+ PTR-ToF-MS are normalized to the primary ion (NO^+) at a level of 10^6 cps to account for fluctuations of the ion source and detector (see Supplement).

Compared to proton transfer reactions occurring mostly between H_3O^+ ions and VOC (volatile organic compound) species, NO^+ ions show a variety of reaction pathways with VOCs, which can be roughly summarized as follows:

– charge transfer

$$NO^+ + MH \rightarrow MH^+ + NO, \quad \text{(R5)}$$

– hydride ion transfer

$$NO^+ + MH \rightarrow M^+ + HNO, \quad \text{(R6)}$$

– association reaction

$$NO^+ + M + N_2 \rightarrow M \bullet \left(NO^+\right) + N_2. \quad \text{(R7)}$$

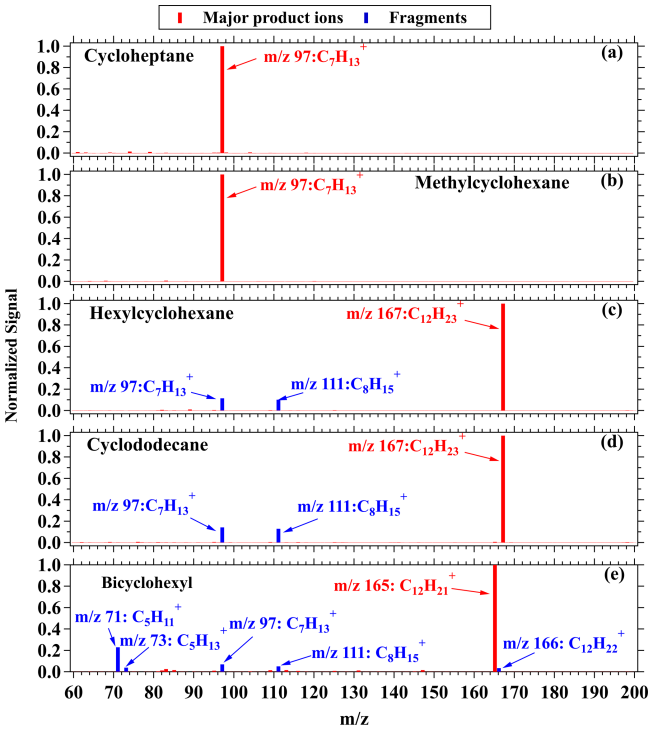

Figure 2. Mass spectra of product ions from cycloheptane **(a)**, methylcyclohexane **(b)**, hexylcyclohexane **(c)**, cyclododecane **(d)**, and bicyclohexyl **(e)** in NO^+ PTR-ToF-MS. The major product ions are shown in red, and the fragments are shown in blue.

As shown in Fig. 1, the ionization energy (IE) of VOC species is a determining factor for the reaction pathways with NO^+. For example, as the IE of NO is 9.26 eV (Reiser et al., 1988), species with an IE less than 9.26 eV, e.g., benzene and isoprene, will undergo charge transfer reaction (Reaction R5) with NO^+ (Španěl and Smith, 1999, 1996), while species with IE greater than 9.26 eV, e.g., acetone and *n*-undecane, will undergo hydride ion transfer (Reaction R6) or association reaction (Reaction R7) with NO^+ (Amador-Muñoz et al., 2016; Diskin et al., 2002; Koss et al., 2016).

2.2 Calibration and correction experiments

In this study, we investigate characteristic ions of cycloalkanes generated by NO^+ ionization from a series of species identification experiments. The information of cycloalkanes species used in these experiments is listed in Table 1. In addition, we also evaluated potential interferences from mono-alkenes, the isomers of cycloalkanes. Calibration experiments were carried out to obtain the sensitivities of cycloalkanes in both the laboratory and the field, using a customized cylinder gas standard (Apel-Riemer Environmental, Inc., USA), containing five different alkyl-cyclohexanes (C_{10}–C_{14}) and eight *n*-alkanes (C_8–C_{15}) (Table S1).

Furthermore, some additional experiments were performed to explore the influence of humidity and tubing delay

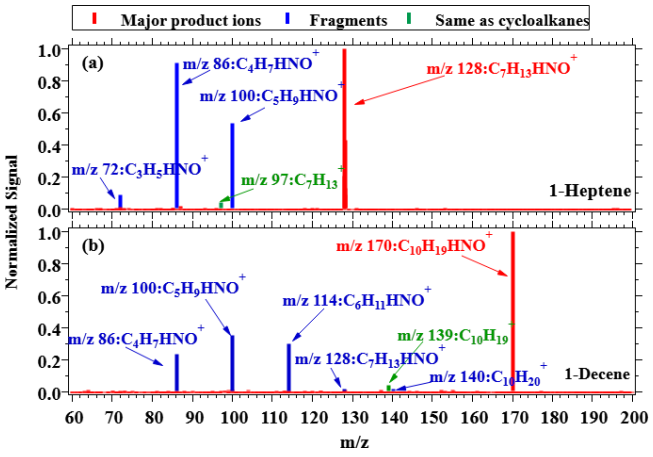

Figure 3. Mass spectra of product ions from 1-heptene **(a)** and 1-decene **(b)** with NO^+ PTR-ToF-MS. The major product ions are shown in red. The same product ions as the cycloalkanes (M–H ions) are shown in green, and other fragments are shown in blue.

effects on measurements of cycloalkanes. Previously, it was shown that response factors of higher alkanes in NO^+ PTR-ToF-MS are slightly affected by air humidity, and the degree of influence is related to carbon number (Wang et al., 2020). Therefore, we evaluate the influence of humidity on sensitivities of cycloalkanes in NO^+ PTR-ToF-MS using a custom-built humidity delivery system (Fig. S4), and the results are applied to explore the relationship between sensitivities of cycloalkanes and humidity. The perfluoroalkoxy (PFA) Teflon tubing is used for inlets in this study, but gas-wall partitioning can be important for low-volatility compounds (Pagonis et al., 2017). As a result, measurements from controlled laboratory experiments and field deployments were analyzed to systematically quantify and characterize the tubing delay time of cycloalkanes.

3 Results and discussion

3.1 Characterization of product ion distribution

NO^+ PTR-ToF-MS was used to directly measure high-purity cycloalkane species and identify the characteristic product ions produced by cycloalkanes under NO^+ ionization. Here, the major product ions, fragments, and their contributions for different cycloalkanes are shown in Table 1. Chemical formulas of the product ions are determined based on the positions of measured mass peaks.

Figure 2 shows mass spectra within the relevant range (m/z 0^+ to 200^+ Th) for cycloalkanes. The signals are normalized to the largest ion peak for better comparison. As shown in Fig. 2, no significant fragmentation appears for cycloheptane and methylcyclohexane (C_7H_{14}), and the dominating product ions are observed at m/z 97 Th, corresponding to $C_7H_{13}^+$. Similarly, the product ions generated by hexyl-

Table 2. Carbon numbers and formulas, mean normalized sensitivities, and detection limits of cycloalkanes in NO^+ PTR-ToF-MS.

Cycloalkanes (C number)	Formula	Normalized sensitivities (ncps ppb^{-1})	Detection limit (ppt)	
			10 s	1 min
C_{10}	$C_{10}H_{20}$	231.3	7.20	3.04
C_{11}	$C_{11}H_{22}$	207.8	7.72	2.76
C_{12}	$C_{12}H_{24}$	223.9	7.01	2.85
C_{13}	$C_{13}H_{26}$	244.6	6.24	2.46
C_{14}	$C_{14}H_{28}$	247.9	6.22	2.40
C_{15}	$C_{15}H_{30}$	N/A[a]	6.67	2.54
C_{16}	$C_{16}H_{32}$	N/A	7.28	2.96
C_{17}	$C_{17}H_{34}$	N/A	7.46	3.05
C_{18}	$C_{18}H_{36}$	N/A	7.90	3.40
C_{19}	$C_{19}H_{38}$	N/A	8.21	3.61
C_{20}	$C_{20}H_{40}$	N/A	8.08	3.48

[a] N/A stands for "not available". The average sensitivity of C_{10}–C_{14} cyclic alkanes was used to predict the concentrations of cyclic alkanes with higher carbon (C_{15}–C_{20}) and bicyclic alkanes (C_{10}–C_{20}).

cyclohexane and cyclododecane ($C_{12}H_{24}$) under NO^+ ionization mainly appear at m/z 167 Th (Fig. 2c–d), corresponding to $C_{12}H_{23}^+$, and fragments occur at m/z 97 Th and m/z 111 Th, corresponding to $C_7H_{13}^+$ and $C_8H_{15}^+$, respectively. The product ions generated by cyclopentadecane and nonylcyclohexane ($C_{15}H_{30}$) mainly appear at m/z 209 Th, corresponding to $C_{15}H_{29}^+$, with slightly more fragmentation than C_{12} cyclic alkanes (Fig. S5). Bicyclic cycloalkanes undergo the same ionization channel from NO^+ ionization, as demonstrated by major product ions at m/z 165 Th ($C_{12}H_{21}^+$) and other fragmentation ions from bicyclohexyl ($C_{12}H_{22}$) (Fig. 2e). For instance, the mass spectra for C_{10}–C_{14} alkylcyclohexanes during the calibration experiments are shown in Fig. S6, with the same $C_nH_{2n-1}^+$ as the major product ions. The fractions of M–H ions generated by high-purity cycloalkane species including C_7, C_{12}, and C_{15} cyclic alkanes and C_{12} bicyclic alkanes are summarized in Fig. S7. We observe that M–H ions account for $\sim 100\,\%$ of total ion signals for C_7 cyclic alkanes and lower but comparable fractions (74 %–82 %) for C_{12} and C_{15} cyclic alkanes. These results verify that reactions of cyclic and bicyclic alkanes with NO^+ ions follow the hydride ion transfer pathway to yield $C_nH_{2n-1}^+$ and $C_nH_{2n-3}^+$ product ions, respectively. As mentioned above, the characteristic peaks of cycloalkanes under NO^+ ionization are consistent with the ions that are received from the attempts to utilize H_3O^+ PTR-MS. For the latter method though, sensitivities are reported to be lower (Erickson et al., 2014; Gueneron et al., 2015; Warneke et al., 2014; Yuan et al., 2014). As the result, we speculate that reactions of NO^+ with cycloalkanes may present large contributions to cycloalkane M–H product ions in the H_3O^+ chemistry mode of PTR-MS (Španěl et al., 1995).

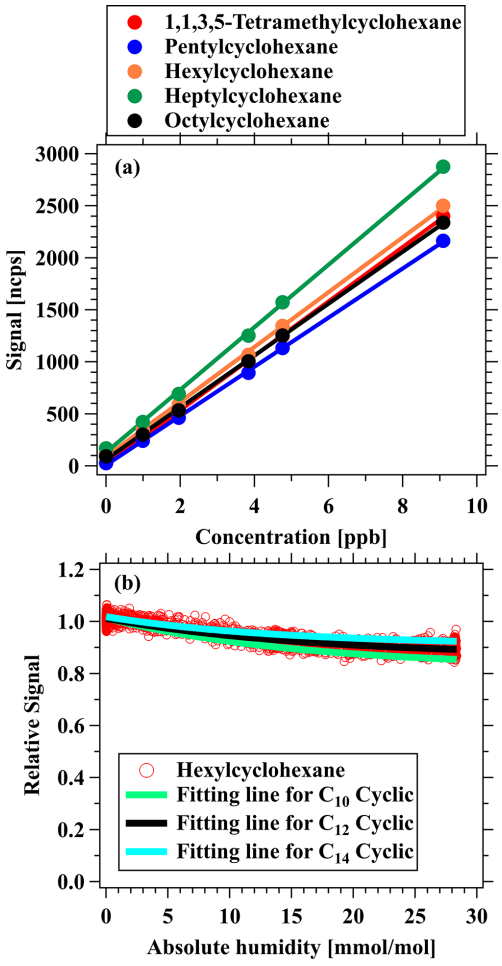

Figure 4. **(a)** Multipoint calibration curve for 1,1,3,5-tetramethylcyclohexane (red), pentylcyclohexane (blue), hexylcyclohexane (orange), heptylcyclohexane (green), and octylcyclohexane (black). **(b)** Humidity dependence of sensitivity for various cycloalkanes, including measurement results for hexylcyclohexane (red markers) and the fitted lines for C_{10} cyclic alkane (green), C_{12} cyclic alkane (black), and C_{14} cyclic alkane (blue), with the corresponding fitted functions of $y = 0.82 + 0.19 \times \exp(-0.06x)$, $y = 0.87 + 0.14 \times \exp(-0.06x)$, and $y = 0.90 + 0.11 \times \exp(-0.07x)$, respectively.

As the isomers of cyclic alkanes, alkenes may interfere with measurements of cycloalkanes. Here, we use 1-heptene (C_7H_{14}) and 1-decene ($C_{10}H_{20}$), the isomers of C_7 and C_{10} cyclic alkanes, to explore the ionization regime of alkenes in NO^+ chemical ionization (Fig. 3 and Table 1). These two alkenes produce more fragments than cycloalkanes under NO^+ chemistry but mainly react with NO^+ via association reactions to yield $C_nH_{2n} \cdot (NO)^+$ product ions. The major product ions of 1-heptene and 1-decene appear at m/z 128 Th and m/z 170 Th, corresponding to $C_7H_{13}HNO^+$ and $C_{10}H_{19}HNO^+$, respectively. Based on the mass spectra, alkenes produce the $C_nH_{2n-1}^+$ product ions at fractions of $< 5\,\%$, which are similar to fragmentation ions from NO^+

ionization of the two species and other 1-alkenes determined from a selected ion flow tube mass spectrometer (SIFT-MS) (Diskin et al., 2002). The same study (Diskin et al., 2002) also demonstrated that *trans*-2-alkenes might produce more $C_nH^+_{2n-1}$ ions under NO^+ ionization (e.g., *trans*-2-heptene contributes 40 % of $C_7H^+_{13}$ ions). However, concentrations of 1-alkenes and *trans*-2-alkenes in the atmosphere are usually significantly lower than cycloalkanes (about 25 % and < 15 %, respectively) (de Gouw et al., 2017; Yuan et al., 2013). We further compare the signals of $C_nH^+_{2n}$ and $C_nH^+_{2n-1}$ from calibration experiments, urban air measurements, and a chassis dynamometer study (Fig. S8). The typical ratios of $C_nH^+_{2n}/C_nH^+_{2n-1}$ for cyclic alkanes are in the range of 2 %–6 %, with similar ratios determined from urban air measurements (3 %–7 %). The ratios of $C_nH^+_{2n}$ to $C_nH^+_{2n-1}$ from vehicular emissions are maintained at 6 %–16 % for C_{10}–C_{14} ions, which is a little bit higher than those determined from cyclic alkanes, while the ratios of C_{15}–C_{20} ions are comparable with pure cyclic alkanes (4 %–8 %). Even though all of these differences are attributed to potential interference from 2-alkenes and assume the same quantity of $C_nH^+_{2n-1}$ and $C_nH^+_{2n}$ ions from NO^+ ionization from 2-alkenes, the upper limits of the interference from alkenes should be in the range of 1 %–2 % for urban air measurements and 2 %–12 % for measurements of vehicular emissions. Therefore, we conclude that the interferences from alkenes to cyclic alkane measurements in most environments are minor.

3.2 Sensitivity, humidity dependence, and detection limits

The calibration experiments of cycloalkanes (see details of gas standard in Table S1) are carried out in both dry conditions (< 1 % RH) and humidified conditions (Fig. S9). Figure 4 illustrates the results from a typical calibration experiment for five different alkyl-substituted cyclohexanes with carbon atoms of 10–14 in dry air (relative humidity < 1 %) for NO^+ PTR-ToF-MS. There is a good linear relationship between ion signals and concentrations of various cycloalkanes ($R = 0.9996$ to 0.9999). Sensitivities (ncps ppb^{-1}) of cycloalkanes are in the range of 210 to 260 ncps ppb^{-1} (Table 2). The sensitivity of each cycloalkane remained stable in the long-term calibration conducted in the laboratory and in the field (Fig. S10). Table 2 further shows the detection limits of cycloalkanes by NO^+ PTR-ToF-MS, which are calculated as the concentrations with a signal-to-noise ratio of 3 (Bertram et al., 2011; Yuan et al., 2017). The detection limits of cycloalkanes at the integral times of 10 s and 1 min are in the range of 6.2–8.2 ppt and 2.4–3.6 ppt, respectively. For comparison, the detection limits of NO^+ PTR-ToF-MS for 24 h of integral time are also determined, obtaining comparable results (< 0.1 ppt) with detection limits of GC × GC-ToF-MS (0.1–0.3 ppt for daily sample) (Liang et al., 2018; Xu et al., 2020a),.

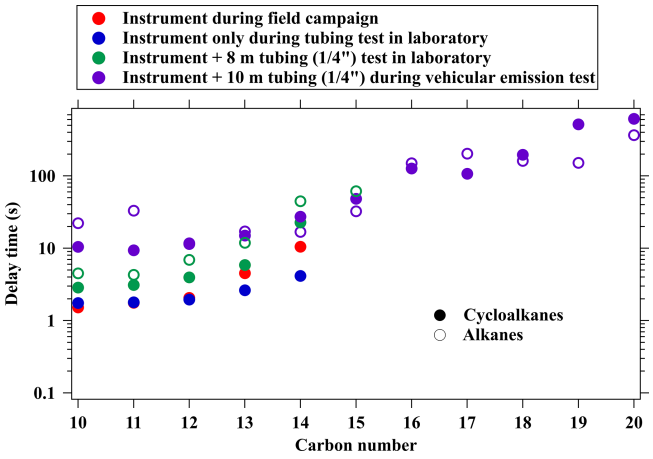

Figure 5. Delay time of cycloalkanes determined from measurements in the field, laboratory experiments, and vehicular emissions. The delay times of alkanes from Wang et al. (2020) are also shown for comparison.

Figure 4b shows that normalized signals of hexylcyclohexane are relative to dry conditions as a function of different humidity. The relative signals of the explored cycloalkanes show a minor decrease (< 10 %) at the highest humidity (∼ 82 % RH at 25°) compared to the dry condition, and the observed changes for cycloalkanes with different carbon numbers are similar, suggesting little influence of humidity on measurements of cycloalkanes. The humidity-dependence curves determined in Fig. 4b are used to correct variations in ambient humidity in the atmosphere.

The response time of various cycloalkanes in the instrument and also the sampling tubing is determined from laboratory experiments (Fig. S11). For the species not in the gas standard, we also take advantage of vehicular emissions measurements associated with high concentrations of cycloalkanes, and the sampling methods are the same as mentioned in T. Li et al. (2021) and Wang et al. (2022b). Here, we use the delay time to determine response of cycloalkanes, which is calculated based on the time it takes for signals to drop to 10 % of their initial value (Fig. S12) (Pagonis et al., 2017). The delay time of cycloalkanes is summarized in Fig. 5. The delay time of various cycloalkanes generally increases with the carbon numbers, ranging from a few seconds to a few minutes, but are lower than determined for those acyclic alkanes within the C_{10}–C_{15} range (Wang et al., 2020). These results suggest that measured variability in cycloalkanes with higher carbon numbers, especially for C_{19}–C_{20} or above, may only be reliable for timescales longer than 10 min.

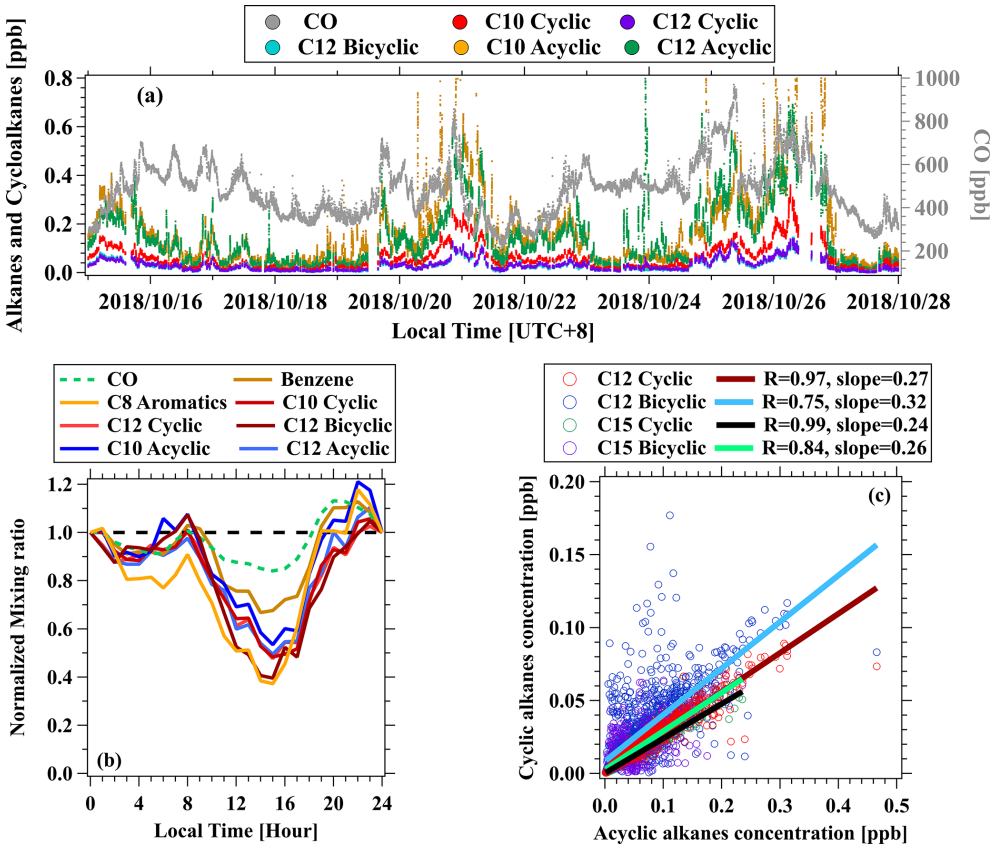

Figure 6. **(a)** Time series of CO, cyclic, bicyclic, and acyclic alkanes measured at the urban site in Guangzhou. **(b)** Normalized diurnal variations in CO, benzene, C_8 aromatics, C_{10} cyclic alkanes, C_{10} acyclic alkanes, C_{12} cyclic alkanes, C_{12} bicyclic alkanes, and C_{12} acyclic alkanes. The measurement data for each species are normalized to midnight concentrations. **(c)** Scatterplots of cyclic and bicyclic alkanes to acyclic alkanes with carbon atoms of 12 and 15.

3.3 Applications in ambient air and vehicular exhausts

Based on the results shown above, we deployed NO^+ PTR-ToF-MS to measure concentration levels and variations in cycloalkanes at an urban site in Guangzhou, southern China. Details of the field campaign have been described in previous studies (Wang et al., 2020; Wu et al., 2020). The average sensitivities of long-term calibration (dry condition) during the field observations were used to quantify cycloalkanes after corrected variations in ambient humidity in the atmosphere. For the cycloalkanes that are not contained in the gas standard, we employ average sensitivity for calibrated cycloalkanes in the gas standard.

The concentration levels and diurnal profiles of cyclic and bicyclic alkanes are illustrated in Fig. 6a, along with CO. In general, cyclic and bicyclic alkanes demonstrated similar temporal variability to CO, suggesting cyclic and bicyclic alkanes may be mainly emitted from primary combustion sources. Concentrations of C_{12} bicyclic alkanes are observed to be comparable with C_{12} cyclic alkanes. As shown in Fig. 6b, selected C_{10} and C_{12} cycloalkanes show diurnal variations with lower concentrations during the daytime. Compared to diurnal variations in other species with different reactivity (Wu et al., 2020), the decline fractions of cycloalkanes are more comparable to the reactive species (e.g., C_8 aromatics) than the inert ones (e.g., CO, benzene), indicating significant daytime photochemical removal of these cycloalkanes. Diurnal patterns of other cyclic and bicyclic alkanes exhibit similar results (Fig. S13). As discussed in Wang et al. (2020), similar diurnal profiles of cycloalkanes with different carbon numbers also imply that the tubing delay effect may not significantly affect temporal variations in cycloalkanes reported here. Based on both time series and correlation analysis (Fig. 6c), cyclic and bicyclic alkanes showed strong correlation with acyclic alkanes, suggesting that they predominantly came from same emission sources.

NO^+ PTR-ToF-MS was also applied to measure cycloalkane emissions along with other organic compounds from vehicles using gasoline, diesel, and liquified petroleum gas (LPG) as fuel, by conducting a chassis dynamometer measurement (Wang et al., 2022b). Figure 7 shows the time series of C_{12} cyclic and bicyclic alkanes, C_{12} alkanes, toluene, and acetaldehyde measured by NO^+ PTR-ToF-MS for a gasoline vehicle with emission standard of China III

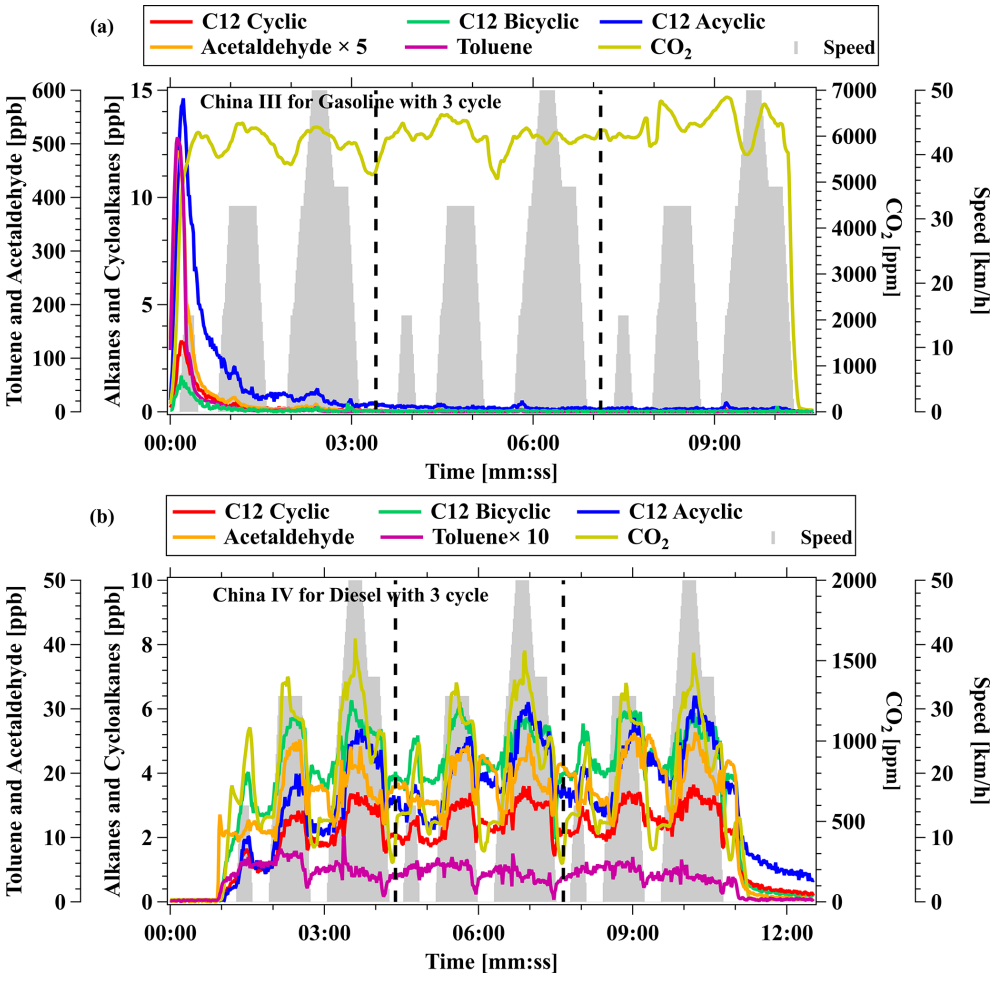

Figure 7. Concentrations of C_{12} cyclic, bicyclic, and acyclic alkanes; acetaldehyde; toluene; and CO_2 for **(a)** a gasoline vehicle with emission standard of China III and **(b)** a diesel vehicle with emission standard of China IV. The gray shadows represent the speeds of the vehicles on the chassis dynamometer. The data of toluene and acetaldehyde were detected by NO^+ PTR-ToF-MS.

and a diesel vehicle with emission standard of China IV. Both test vehicles were started with hot engines. As shown in Fig. 7a, high concentrations of selected cycloalkanes emitted by the gasoline vehicle were observed as the engine started. Compared with typical VOCs exhausted by vehicles (e.g., toluene and acetaldehyde), concentrations of cycloalkanes were lower but showed similar temporal variations. In comparison, cycloalkane emissions from diesel vehicles are obviously different. As shown in Fig. 7b, concentrations of cycloalkanes showed relatively moderate enhancements as the engine started but were significantly enhanced with high vehicle speed, obtaining periodic pattern variations within each test cycle. Though the highest concentrations of cycloalkanes observed for gasoline and diesel vehicles are similar, determined emission factors of diesel vehicles are significantly higher than gasoline vehicles, since emissions of cycloalkanes are mainly concentrated during a short period at the engine start for gasoline vehicles, whereas emissions of cycloalkanes remain high during hot running for diesel vehicles. For instance, the determined emission factors of C_{12} cyclic alkanes are 0.06 mg km^{-1} for gasoline vehicles and 1.17 mg km^{-1} for diesel vehicles. In addition to cycloalkanes and alkanes, other compounds including aromatics and oxygenated VOCs also demonstrate large differences between gasoline and diesel vehicles, which were mainly attributed to different chemical compositions of gasoline and diesel fuels (Wang et al., 2022b). Recent studies reported that cyclic compounds occupied a large proportion of IVOCs emitted from vehicles, with prominent SOA formation potentials (Fang et al., 2021; Huang et al., 2018; Zhao et al., 2016), but emissions of individual cycloalkanes have not been not reported yet. As a result, high-time-resolution measurements of cycloalkanes from vehicular emissions by NO^+ PTR-ToF-MS can improve the characterization of the emission mechanisms of these species.

3.4 Insights from simultaneous measurements of cycloalkanes and alkanes

Since NO^+ PTR-ToF-MS can provide simultaneous measurements of cycloalkanes and acyclic alkanes, we can use this information to explore the relative importance of cycloalkanes. Figure 8 shows mean concentrations of cycloalkanes (cyclic and bicyclic) and alkanes with different carbon numbers (C_{10}–C_{20}) measured by NO^+ PTR-ToF-MS in urban air and emissions from diesel vehicles. In the urban region, concentrations of cyclic and bicyclic cycloalkanes are comparable but lower than acyclic alkanes, with concentration ratios relative to acyclic alkanes in the range of 0.30–0.46 for cyclic alkanes and 0.23–0.51 for bicyclic alkanes. Similar results are obtained for gasoline vehicles, with cyclic alkanes / acyclic alkanes and bicyclic alkanes / acyclic alkanes ratios of 0.27–0.53 and 0.21–0.52, respectively (Fig. 8). The contributions of cycloalkanes in diesel vehicular emissions are relatively high, with the concentration ratios relative to acyclic alkanes in the range of 0.42–0.66 for cyclic alkanes and 0.37–0.95 for bicyclic alkanes.

As there are only limited measurements of bicyclic alkanes in the literature, we compare concentration ratios of cyclic alkanes to acyclic alkanes with results in previous studies, mainly using gas chromatography techniques (GC-MS/FID and GC × GC). The details of the technique used in these earlier studies are summarized in Table S2. As shown in Fig. 9, the ratios obtained in the urban region of Guangzhou in this work (0.2–0.4) are similar to other measurements in urban areas, including Algiers, Algeria (Yassaa et al., 2001). The ratios obtained in London, UK (Xu et al., 2020b), are higher than the ratios obtained in Guangzhou but similar to the diesel exhaust in our work for the C_{13}–C_{18} range. These results are likely due to the fact that the measurement location in London is in close proximity to a main road; cyclic and acyclic alkanes may be dominated by traffic emissions with high fractions of diesel vehicles in fleets. Although some variations are observed in different urban environments, these ratios are broadly within the range between gasoline and diesel emissions. As for emissions from diesel vehicles, the ratios measured in this study are similar to GC × GC measurements in the UK (Alam et al., 2016) for the C_{12}–C_{14} range and GC-MS measurements in the USA (Gentner et al., 2012), whereas the ratios from this study are higher than in Alam et al. (2016) for larger carbon numbers. The relative fractions of cycloalkanes measured from oil and gas regions (Gilman et al., 2013) and emissions from lubricating oil (Liang et al., 2018) (> 0.7) are higher than ambient air and vehicular emissions. The variability pattern of ratios of cyclic alkanes to acyclic alkanes for different carbon numbers may be used for a source analysis of these IVOCs in the future.

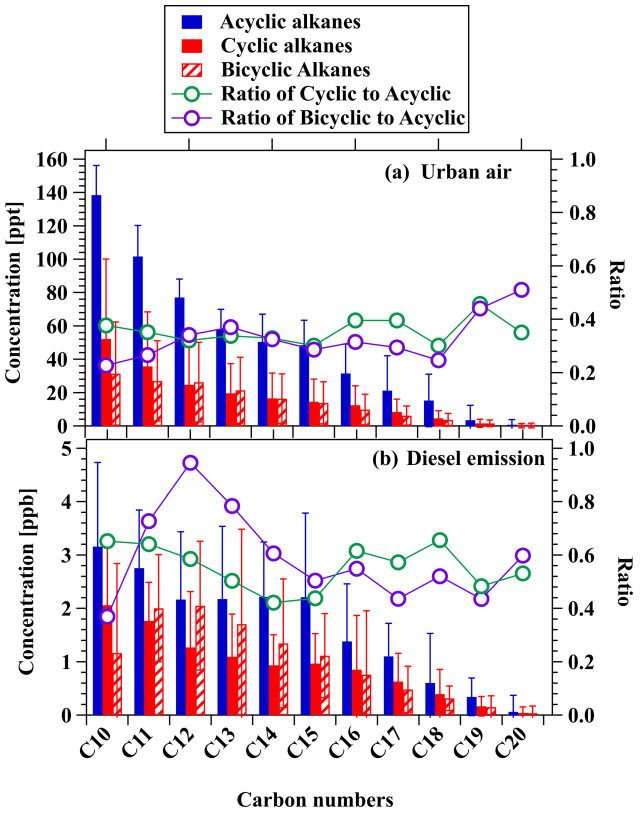

Figure 8. Mean concentrations of cyclic and bicyclic alkanes and alkanes (branched + linear) with different carbon numbers measured by NO^+ PTR-ToF-MS in the urban air **(a)** and diesel emissions **(b)**. The green and purple lines with circles represent the ratios of cyclic and bicyclic alkanes, respectively, to acyclic alkanes under the same carbon numbers. Error bars represent standard deviations of the concentration for the acyclic, cyclic, and bicyclic alkanes.

4 Conclusions

In this study, we show that online measurements of cycloalkanes can be achieved using proton transfer reaction time-of-flight mass spectrometry with NO^+ chemical ionization (NO^+ PTR-ToF-MS). Our results demonstrate that cyclic and bicyclic alkanes are ionized via hydride ion transfer, leading to characteristic product ions of $C_nH^+_{2n-1}$ and $C_nH^+_{2n-3}$, respectively. As isomers of cycloalkanes, alkenes undergo association reactions mainly yielding product ions $C_nH_{2n} \cdot (NO)^+$, which induce little interference with cycloalkane detection. Calibrations of various cycloalkanes show similar sensitivities with low humidity dependence. The detection limits of cycloalkanes are in the range of 2–4 ppt at the integral time of 1 min.

Applying this method, cycloalkanes were successfully measured at an urban site in southern China and in a chassis dynamometer study for vehicular emissions. Concentrations of both cyclic and bicyclic alkanes are substantial in urban air and vehicular emissions. Diurnal variations in cy-

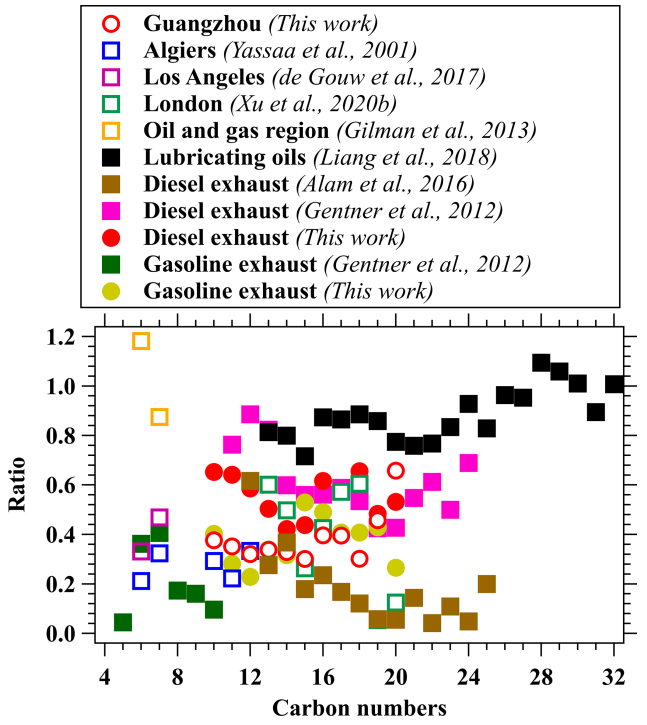

Figure 9. The concentration ratios of cyclic alkanes to acyclic alkanes for different carbon numbers. Measurements in various urban areas, including Guangzhou in China, London in the UK (Xu et al., 2020b), Los Angeles in the USA (de Gouw et al., 2017), Algiers in Algeria (Yassaa et al., 2001), and an oil and gas region in Colorado in the USA (Gilman et al., 2013), are also shown for comparison. Emission sources, including vehicle exhausts (Alam et al., 2016; Gentner et al., 2012) and lubricating oils (Liang et al., 2018), are also included.

cloalkanes in the urban air indicate significant losses due to photochemical processes during the daytime. The concentration ratios of cyclic alkanes to acyclic alkanes are similar between urban air and gasoline vehicle emissions but higher for diesel vehicles, which could potentially be used for source analysis in future studies. Our work demonstrates that NO^+ PTR-ToF-MS provides a new complementary approach for the fast characterization of cycloalkanes in both ambient air and emission sources, which can be helpful to investigate sources of cycloalkanes and their contribution to SOA formation in the atmosphere. Measurements of cycloalkanes in the particle phase may also be possible by combining NO^+ PTR-ToF-MS with "chemical analysis of aerosols online" (CHARON) or other similar aerosol inlets (Muller et al., 2017), which could further provide particle-phase information of cycloalkanes and gas-partitioning analysis of cycloalkanes.

Data availability. Data are available from the authors upon request.

Supplement. The supplement related to this article is available online at: https://doi.org/10.5194/amt-15-6935-2022-supplement.

Author contributions. BY designed the research. YBC, CMW, SHW, XJH, CHW, XS, YBH, XBL, YJL, and MS contributed to data collection. YBC performed data analysis, with contributions from CMW, SHW, XJH, and CHW. YBC and BY prepared the article with contributions from other authors. All the authors reviewed the article.

Competing interests. The contact author has declared that none of the authors has any competing interests.

Disclaimer. Publisher's note: Copernicus Publications remains neutral with regard to jurisdictional claims in published maps and institutional affiliations.

Acknowledgements. The authors gratefully acknowledge the science team for their technical support and discussions during the campaigns and appreciate valuable comments from the three anonymous reviewers.

Financial support. This work was supported by the National Natural Science Foundation of China (grant nos. 42121004, 41877302, 42275103, 42230701) and Guangdong Innovative and Entrepreneurial Research Team Program (grant no. 2016ZT06N263). This work was also supported by the Special Fund Project for Science and Technology Innovation Strategy of Guangdong Province (grant no. 2019B121205004).

Review statement. This paper was edited by Mingjin Tang and reviewed by three anonymous referees.

References

Aklilu, Y.-A., Cho, S., Zhang, Q., and Taylor, E.: Source apportionment of volatile organic compounds measured near a cold heavy oil production area, Atmos. Res., 206, 75–86, 2018.

Alam, M. S., Zeraati-Rezaei, S., Stark, C. P., Liang, Z., Xu, H., and Harrison, R. M.: The characterisation of diesel exhaust particles – composition, size distribution and partitioning, Farad. Discuss., 189, 69–84, 2016.

Alam, M. S., Zeraati-Rezaei, S., Liang, Z., Stark, C., Xu, H., MacKenzie, A. R., and Harrison, R. M.: Mapping and quantifying isomer sets of hydrocarbons ($\geq C_{12}$) in diesel exhaust, lubricating oil and diesel fuel samples using GC × GC-ToF-MS, Atmos. Meas. Tech., 11, 3047–3058, https://doi.org/10.5194/amt-11-3047-2018, 2018.

Amador-Muñoz, O., Misztal, P. K., Weber, R., Worton, D. R., Zhang, H., Drozd, G., and Goldstein, A. H.: Sensitive detection of *n*-alkanes using a mixed ionization mode proton-transfer-

reaction mass spectrometer, Atmos. Meas. Tech., 9, 5315–5329, https://doi.org/10.5194/amt-9-5315-2016, 2016.

Bertram, T. H., Kimmel, J. R., Crisp, T. A., Ryder, O. S., Yatavelli, R. L. N., Thornton, J. A., Cubison, M. J., Gonin, M., and Worsnop, D. R.: A field-deployable, chemical ionization time-of-flight mass spectrometer, Atmos. Meas. Tech., 4, 1471–1479, https://doi.org/10.5194/amt-4-1471-2011, 2011.

de Gouw, J. and Warneke, C.: Measurements of volatile organic compounds in the earth's atmosphere using proton-transfer-reaction mass spectrometry, Mass Spectrom. Rev., 26, 223–257, 2007.

de Gouw, J. A.: Budget of organic carbon in a polluted atmosphere: Results from the New England Air Quality Study in 2002, J. Geophys. Res., 110, D16305, https://doi.org/10.1029/2004JD005623, 2005.

de Gouw, J. A., Gilman, J. B., Kim, S. W., Lerner, B. M., Isaacman-VanWertz, G., McDonald, B. C., Warneke, C., Kuster, W. C., Lefer, B. L., Griffith, S. M., Dusanter, S., Stevens, P. S., and Stutz, J.: Chemistry of Volatile Organic Compounds in the Los Angeles basin: Nighttime Removal of Alkenes and Determination of Emission Ratios, J. Geophys. Res.-Atmos., 122, 11843–811861, 2017.

Diskin, A. M., Wang, T. S., Smith, D., and Spanel, P.: A selected ion flow tube (SIFT), study of the reactions of H_3O^+, NO^+ and O_2^+ ions with a series of alkenes; in support of SIFT-MS, Int. J. Mass Spectrom., 218, 87–101, 2002.

Donahue, N. M., Kroll, J. H., Pandis, S. N., and Robinson, A. L.: A two-dimensional volatility basis set – Part 2: Diagnostics of organic-aerosol evolution, Atmos. Chem. Phys., 12, 615–634, https://doi.org/10.5194/acp-12-615-2012, 2012.

Erickson, M. H., Gueneron, M., and Jobson, B. T.: Measuring long chain alkanes in diesel engine exhaust by thermal desorption PTR-MS, Atmos. Meas. Tech., 7, 225–239, https://doi.org/10.5194/amt-7-225-2014, 2014.

Fang, H., Huang, X., Zhang, Y., Pei, C., Huang, Z., Wang, Y., Chen, Y., Yan, J., Zeng, J., Xiao, S., Luo, S., Li, S., Wang, J., Zhu, M., Fu, X., Wu, Z., Zhang, R., Song, W., Zhang, G., Hu, W., Tang, M., Ding, X., Bi, X., and Wang, X.: Measurement report: Emissions of intermediate-volatility organic compounds from vehicles under real-world driving conditions in an urban tunnel, Atmos. Chem. Phys., 21, 10005–10013, https://doi.org/10.5194/acp-21-10005-2021, 2021.

Federer, W., Dobler, W., Howorka, F., Lindinger, W., Durup-Ferguson, M., and Ferguson, E. E.: Collisional relaxation of vibrationally excited $NO^+(v)$ ions, The J. Chem. Phys., 83, 1032–1038, 1985.

Gentner, D. R., Isaacman, G., Worton, D. R., Chan, A. W., Dallmann, T. R., Davis, L., Liu, S., Day, D. A., Russell, L. M., Wilson, K. R., Weber, R., Guha, A., Harley, R. A., and Goldstein, A. H.: Elucidating secondary organic aerosol from diesel and gasoline vehicles through detailed characterization of organic carbon emissions, P. Natl. Acad. Sci. USA, 109, 18318–18323, 2012.

Gilman, J. B., Lerner, B. M., Kuster, W. C., and de Gouw, J. A.: Source Signature of Volatile Organic Compounds from Oil and Natural Gas Operations in Northeastern Colorado, Environ. Sci. Technol., 47, 1297–1305, 2013.

Goldstein, A. H. and Galbally, I. E.: Known and unknown organic constituents in the Earth' s atmosphere, Environ. Sci. Technol., 41, 1514–1521, 2007.

Gueneron, M., Erickson, M. H., VanderSchelden, G. S., and Jobson, B. T.: PTR-MS fragmentation patterns of gasoline hydrocarbons, Int. J. Mass Spectro., 379, 97–109, 2015.

He, X., Yuan, B., Wu, C., Wang, S., Wang, C., Huangfu, Y., Qi, J., Ma, N., Xu, W., Wang, M., Chen, W., Su, H., Cheng, Y., and Shao, M.: Volatile organic compounds in wintertime North China Plain: Insights from measurements of proton transfer reaction time-of-flight mass spectrometer (PTR-ToF-MS), J. Environ. Sci., 114, 98–114, 2022.

Hu, W., Zhou, H., Chen, W., Ye, Y., Pan, T., Wang, Y., Song, W., Zhang, H., Deng, W., Zhu, M., Wang, C., Wu, C., Ye, C., Wang, Z., Yuan, B., Huang, S., Shao, M., Peng, Z., Day, D. A., Campuzano-Jost, P., Lambe, A. T., Worsnop, D. R., Jimenez, J. L., and Wang, X.: Oxidation Flow Reactor Results in a Chinese Megacity Emphasize the Important Contribution of S/IVOCs to Ambient SOA Formation, Environ. Sci. Technol., 56, 6880–6893, 2022.

Huang, C., Hu, Q., Li, Y., Tian, J., Ma, Y., Zhao, Y., Feng, J., An, J., Qiao, L., Wang, H., Jing, S. A., Huang, D., Lou, S., Zhou, M., Zhu, S., Tao, S., and Li, L.: Intermediate Volatility Organic Compound Emissions from a Large Cargo Vessel Operated under Real-World Conditions, Environ. Sci. Technol., 52, 12934–12942, 2018.

Hunter, J. F., Carrasquillo, A. J., Daumit, K. E., and Kroll, J. H.: Secondary organic aerosol formation from acyclic, monocyclic, and polycyclic alkanes, Environ. Sci. Technol., 48, 10227–10234, 2014.

Inomata, S., Tanimoto, H., and Yamada, H.: Mass Spectrometric Detection of Alkanes Using NO+ Chemical Ionization in Proton-transfer-reaction Plus Switchable Reagent Ion Mass Spectrometry, Chem. Lett., 43, 538–540, 2014.

Jahn, L. G., Wang, D. S., Dhulipala, S. V., and Ruiz, L. H.: Gas-Phase Chlorine Radical Oxidation of Alkanes: Effects of Structural Branching, NOx, and Relative Humidity Observed during Environmental Chamber Experiments, The J. Phys. Chem. A, 125, 7303–7317, 2021.

Karl, T., Hansel, A., Cappellin, L., Kaser, L., Herdlinger-Blatt, I., and Jud, W.: Selective measurements of isoprene and 2-methyl-3-buten-2-ol based on NO^+ ionization mass spectrometry, Atmos. Chem. Phys., 12, 11877–11884, https://doi.org/10.5194/acp-12-11877-2012, 2012.

Koss, A., Yuan, B., Warneke, C., Gilman, J. B., Lerner, B. M., Veres, P. R., Peischl, J., Eilerman, S., Wild, R., Brown, S. S., Thompson, C. R., Ryerson, T., Hanisco, T., Wolfe, G. M., Clair, J. M. St., Thayer, M., Keutsch, F. N., Murphy, S., and de Gouw, J.: Observations of VOC emissions and photochemical products over US oil- and gas-producing regions using high-resolution H3O+ CIMS (PTR-ToF-MS), Atmos. Meas. Tech., 10, 2941–2968, https://doi.org/10.5194/amt-10-2941-2017, 2017.

Koss, A. R., Warneke, C., Yuan, B., Coggon, M. M., Veres, P. R., and de Gouw, J. A.: Evaluation of NO^+ reagent ion chemistry for online measurements of atmospheric volatile organic compounds, Atmos. Meas. Tech., 9, 2909–2925, https://doi.org/10.5194/amt-9-2909-2016, 2016.

Li, J., Wang, W., Li, K., Zhang, W., Peng, C., Liu, M., Chen, Y., Zhou, L., Li, H., and Ge, M.: Effect of chemical structure on optical properties of secondary organic aerosols derived from C12 alkanes, Sci. Total Environ., 751, 141620, 2021.

Li, T., Wang, Z., Yuan, B., Ye, C., Lin, Y., Wang, S., Sha, Q. e., Yuan, Z., Zheng, J., and Shao, M.: Emissions of carboxylic acids, hydrogen cyanide (HCN) and isocyanic acid (HNCO) from vehicle exhaust, Atmos. Environ., 247, 118218, 2021.

Li, Y., Ren, B., Qiao, Z., Zhu, J., Wang, H., Zhou, M., Qiao, L., Lou, S., Jing, S., Huang, C., Tao, S., Rao, P., and Li, J.: Characteristics of atmospheric intermediate volatility organic compounds (IVOCs) in winter and summer under different air pollution levels, Atmos. Environ., 210, 58–65, 2019.

Liang, Z., Chen, L., Alam, M. S., Zeraati Rezaei, S., Stark, C., Xu, H., and Harrison, R. M.: Comprehensive chemical characterization of lubricating oils used in modern vehicular engines utilizing GC×GC-TOFMS, Fuel, 220, 792–799, 2018.

Lim, Y. B. and Ziemann, P. J.: Effects of Molecular Structure on Aerosol Yields from OH Radical-Initiated Reactions of Linear, Branched, and Cyclic Alkanes in the Presence of NO_x, Environ. Sci. Technol., 43, 2328–2334, 2009.

Lou, H., Hao, Y., Zhang, W., Su, P., Zhang, F., Chen, Y., Feng, D., and Li, Y.: Emission of intermediate volatility organic compounds from a ship main engine burning heavy fuel oil, J. Environ. Sci., 84, 197–204, 2019.

Loza, C. L., Craven, J. S., Yee, L. D., Coggon, M. M., Schwantes, R. H., Shiraiwa, M., Zhang, X., Schilling, K. A., Ng, N. L., Canagaratna, M. R., Ziemann, P. J., Flagan, R. C., and Seinfeld, J. H.: Secondary organic aerosol yields of 12-carbon alkanes, Atmos. Chem. Phys., 14, 1423–1439, https://doi.org/10.5194/acp-14-1423-2014, 2014.

Monks, P. S., Archibald, A. T., Colette, A., Cooper, O., Coyle, M., Derwent, R., Fowler, D., Granier, C., Law, K. S., Mills, G. E., Stevenson, D. S., Tarasova, O., Thouret, V., von Schneidemesser, E., Sommariva, R., Wild, O., and Williams, M. L.: Tropospheric ozone and its precursors from the urban to the global scale from air quality to short-lived climate forcer, Atmos. Chem. Phys., 15, 8889–8973, https://doi.org/10.5194/acp-15-8889-2015, 2015.

Muller, M., Eichler, P., D'Anna, B., Tan, W., and Wisthaler, A.: Direct Sampling and Analysis of Atmospheric Particulate Organic Matter by Proton-Transfer-Reaction Mass Spectrometry, Anal Chem., 89, 10889–10897, 2017.

Pagonis, D., Krechmer, J. E., de Gouw, J., Jimenez, J. L., and Ziemann, P. J.: Effects of gas–wall partitioning in Teflon tubing and instrumentation on time-resolved measurements of gas-phase organic compounds, Atmos. Meas. Tech., 10, 4687–4696, https://doi.org/10.5194/amt-10-4687-2017, 2017.

Reiser, G., Habenicht, W., Müller-Dethlefs, K., and Schlag, E. W.: The ionization energy of nitric oxide, Chem. Phys. Lett., 152, 119–123, 1988.

Robinson, A. L., Donahue, N. M., Shrivastava, M. K., Weitkamp, E. A., Sage, A. M., Grieshop, A. P., Lane, T. E., Pierce, J. R., and Pandis, S. N.: Rethinking Organic Aerosols: Semivolatile Emissions and Photochemical Aging, Science, 315, 1259–1262, 2007.

Španěl, P. and Smith, D.: A selected ion flow tube study of the reactions of $NO^+$and O_2^+ ions with some organic molecules: The potential for trace gas analysis of air, The J. Chem. Phys., 104, 1893–1899, 1996.

Španěl, P. and Smith, D.: Selected ion flow tube studies of the reactions of H_3O^+, NO^+, and O_2^+ with several aromatic and aliphatic monosubstituted halocarbons, Int. J. Mass Spectrom., 189, 213–223, 1999.

Španěl, P., Pavlik, M., and Smith, D.: Reactions of H_3O^+ and OH^- ions with some organic molecules; applications to trace gas analysis in air, Int. J. Mass Spectrom. Ion Process., 145, 177–186, 1995.

Stark, H., Yatavelli, R. L. N., Thompson, S. L., Kimmel, J. R., Cubison, M. J., Chhabra, P. S., Canagaratna, M. R., Jayne, J. T., Worsnop, D. R., and Jimenez, J. L.: Methods to extract molecular and bulk chemical information from series of complex mass spectra with limited mass resolution, Int. J. Mass Spectrom., 389, 26–38, 2015.

Sulzer, P., Hartungen, E., Hanel, G., Feil, S., Winkler, K., Mutschlechner, P., Haidacher, S., Schottkowsky, R., Gunsch, D., Seehauser, H., Striednig, M., Jürschik, S., Breiev, K., Lanza, M., Herbig, J., Märk, L., Märk, T. D., and Jordan, A.: A Proton Transfer Reaction-Quadrupole interface Time-Of-Flight Mass Spectrometer (PTR-QiTOF): High speed due to extreme sensitivity, Int. J. Mass Spectrom., 368, 1–5, 2014.

Timonen, H., Cubison, M., Aurela, M., Brus, D., Lihavainen, H., Hillamo, R., Canagaratna, M., Nekat, B., Weller, R., Worsnop, D., and Saarikoski, S.: Applications and limitations of constrained high-resolution peak fitting on low resolving power mass spectra from the ToF-ACSM, Atmos. Meas. Tech., 9, 3263–3281, https://doi.org/10.5194/amt-9-3263-2016, 2016.

Tkacik, D. S., Presto, A. A., Donahue, N. M., and Robinson, A. L.: Secondary Organic Aerosol Formation from Intermediate-Volatility Organic Compounds: Cyclic, Linear, and Branched Alkanes, Environ. Sci. Technol., 46, 8773–8781, 2012.

Wang, C., Yuan, B., Wu, C., Wang, S., Qi, J., Wang, B., Wang, Z., Hu, W., Chen, W., Ye, C., Wang, W., Sun, Y., Wang, C., Huang, S., Song, W., Wang, X., Yang, S., Zhang, S., Xu, W., Ma, N., Zhang, Z., Jiang, B., Su, H., Cheng, Y., Wang, X., and Shao, M.: Measurements of higher alkanes using NO+ chemical ionization in PTR-ToF-MS: important contributions of higher alkanes to secondary organic aerosols in China, Atmos. Chem. Phys., 20, 14123–14138, https://doi.org/10.5194/acp-20-14123-2020, 2020.

Wang, K., Wang, W., Fan, C., Li, J., Lei, T., Zhang, W., Shi, B., Chen, Y., Liu, M., Lian, C., Wang, Z., and Ge, M.: Reactions of C12-C14 n-Alkylcyclohexanes with Cl Atoms: Kinetics and Secondary Organic Aerosol Formation, Environ. Sci. Technol., 56, 4859–4870, 2022a.

Wang, S., Yuan, B., Wu, C., Wang, C., Li, T., He, X., Huangfu, Y., Qi, J., Li, X.-B., Sha, Q., Zhu, M., Lou, S., Wang, H., Karl, T., Graus, M., Yuan, Z., and Shao, M.: Oxygenated volatile organic compounds (VOCs) as significant but varied contributors to VOC emissions from vehicles, Atmos. Chem. Phys., 22, 9703–9720, https://doi.org/10.5194/acp-22-9703-2022, 2022b.

Warneke, C., Geiger, F., Edwards, P. M., Dube, W., Pétron, G., Kofler, J., Zahn, A., Brown, S. S., Graus, M., Gilman, J. B., Lerner, B. M., Peischl, J., Ryerson, T. B., de Gouw, J. A., and Roberts, J. M.: Volatile organic compound emissions from the oil and natural gas industry in the Uintah Basin, Utah: oil and gas well pad emissions compared to ambient air composition, Atmos. Chem. Phys., 14, 10977–10988, https://doi.org/10.5194/acp-14-10977-2014, 2014.

Wu, C., Wang, C., Wang, S., Wang, W., Yuan, B., Qi, J., Wang, B., Wang, H., Wang, C., Song, W., Wang, X., Hu, W., Lou, S., Ye, C., Peng, Y., Wang, Z., Huangfu, Y., Xie, Y., Zhu, M., Zheng, J., Wang, X., Jiang, B., Zhang, Z., and Shao, M.: Mea-

surement report: Important contributions of oxygenated compounds to emissions and chemistry of volatile organic compounds in urban air, Atmos. Chem. Phys., 20, 14769–14785, https://doi.org/10.5194/acp-20-14769-2020, 2020.

Xing, L. Q., Wang, L. C., and Zhang, R.: Characteristics and health risk assessment of volatile organic compounds emitted from interior materials in vehicles: a case study from Nanjing, China, Environ. Sci. Pollut. Res., 25, 14789–14798, 2018.

Xu, R., Alam, M. S., Stark, C., and Harrison, R. M.: Behaviour of traffic emitted semi-volatile and intermediate volatility organic compounds within the urban atmosphere, Sci. Total Environ., 720, 137470, 2020a.

Xu, R., Alam, M. S., Stark, C., and Harrison, R. M.: Composition and emission factors of traffic- emitted intermediate volatility and semi-volatile hydrocarbons (C_{10}–C_{36}) at a street canyon and urban background sites in central London, UK, Atmos. Environ., 231, 117448, 2020b.

Yassaa, N., Meklati, B. Y., Brancaleoni, E., Frattoni, M., and Cecchioli, P.: Polar and non-polar volatile organic compounds (VOCs) in urban Algiers and saharian sites of Algeria, Atmos. Environ., 35, 787–801, 2001.

Yee, L. D., Craven, J. S., Loza, C. L., Schilling, K. A., Ng, N. L., Canagaratna, M. R., Ziemann, P. J., Flagan, R. C., and Seinfeld, J. H.: Effect of chemical structure on secondary organic aerosol formation from C_{12} alkanes, Atmos. Chem. Phys., 13, 11121–11140, https://doi.org/10.5194/acp-13-11121-2013, 2013.

Yuan, B., Hu, W. W., Shao, M., Wang, M., Chen, W. T., Lu, S. H., Zeng, L. M., and Hu, M.: VOC emissions, evolutions and contributions to SOA formation at a receptor site in eastern China, Atmos. Chem. Phys., 13, 8815–8832, https://doi.org/10.5194/acp-13-8815-2013, 2013.

Yuan, B., Warneke, C., Shao, M., and de Gouw, J. A.: Interpretation of volatile organic compound measurements by proton-transfer-reaction mass spectrometry over the deepwater horizon oil spill, Int. J. Mass Spectrom., 358, 43–48, 2014.

Yuan, B., Koss, A. R., Warneke, C., Coggon, M., Sekimoto, K., and de Gouw, J. A.: Proton-Transfer-Reaction Mass Spectrometry: Applications in Atmospheric Sciences, Chem. Rev., 117, 13187–13229, 2017.

Zhao, Y., Hennigan, C. J., May, A. A., Tkacik, D. S., De Gouw, J. A., Gilman, J. B., Kuster, W. C., Borbon, A., and Robinson, A. L.: Intermediate-Volatility Organic Compounds: A Large Source of Secondary Organic Aerosol, Environ. Sci. Technol., 48, 13743–13750, 2014.

Zhao, Y., Nguyen, N. T., Presto, A. A., Hennigan, C. J., May, A. A., and Robinson, A. L.: Intermediate Volatility Organic Compound Emissions from On-Road Diesel Vehicles: Chemical Composition, Emission Factors, and Estimated Secondary Organic Aerosol Production, Environ. Sci. Technol., 49, 11516–11526, 2015.

Zhao, Y., Nguyen, N. T., Presto, A. A., Hennigan, C. J., May, A. A., and Robinson, A. L.: Intermediate Volatility Organic Compound Emissions from On-Road Gasoline Vehicles and Small Off-Road Gasoline Engines, Environ. Sci. Technol., 50, 4554–4563, 2016.